EAST EUROPEAN JOURNAL OF PHYSICS. 1. 286-292 (2026)
DOI:10.26565/2312-4334-2026-1-33 ISSN 2312-4334

PHOTOELECTRIC PROPERTIES OF $Zn_xCd_{1-x}S$-BASED PHOTOSENSITIVE SEMICONDUCTOR STRUCTURES WITH ENHANCED ULTRAVIOLET RESPONSE

R.R. Kabulov[1], D.B. Istamov[1]*, K.T. Suyarov[2], F.A. Akbarov[3]
[1]*Physical-Technical Institute of Uzbekistan Academy of Sciences, Tashkent 100084, Uzbekistan*
[2]*Chirchik State Pedagogical University, 111700 Chirchik, Uzbekistan*
[3]*Tashkent State Technical University, 100095 Tashkent, Uzbekistan*
**Corresponding Author e-mail: istamov@uzsci.net*
Received September 19, 2025. revised January 26, 2026; accepted January 30, 2026

The work is devoted to the study of the photoelectric properties of $Au - Zn_xCd_{1-x}S - Mo$ structured films, which are photosensitive in the ultraviolet and visible regions of the electromagnetic spectrum, with maximum sensitivity in the ultraviolet region. It has been established that the spectral response of the $Au - Zn_xCd_{1-x}S - Mo$ structured films depend on the temperatures of the ZnS and CdS evaporators, which influence the composition of the photoactive $Zn_xCd_{1-x}S$ layer ($x = Zn/(Zn + Cd)$). By varying the temperature of the ZnS evaporator during the growth of the $Zn_xCd_{1-x}S$ layer, a graded $Zn_xCd_{1-x}S$ film was synthesized on a molybdenum substrate, forming the photoactive layer of the structure. The resulting photosensitive structure exhibited sensitivity in both the ultraviolet and visible regions, with a maximum in the ultraviolet. Analysis of the spectral response indicates that the photoactive layer has a graded band gap, decreasing from $E_G = 3.05 \pm 0.05\ eV$ to $E_G = 2.45 \pm 0.05\ eV$. A study of light current-voltage characteristics for monochromatic radiation showed that they are characterized by different values of the diode ideality factor (n) and reverse saturation current (J_0). The synthesized $Zn_xCd_{1-x}S$ layer can be used as a buffer layer in thin-film solar cells, such as $CdTe, CIGS$ and others, instead of the CdS layer, which will enable increasing both the short-circuit current and the open-circuit voltage of thin-film solar cells.
Keywords: *Polycrystalline films; $Zn_xCd_{1-x}S$; Spectral sensitivity; Photoelectric characteristics; Solar cells; Short circuit current; Open circuit voltage*
PACS: 72.40.+w, 73.50.Pz, 73.61.Ga, 78.40.Fy, 85.60.Dw, 88.40.hj

INTRODUCTION

Currently, the rapid development of automation in the manufacturing process and the production of environmentally friendly electric energy, achieved by directly converting solar energy into electricity, necessitates the use of semiconductor materials that are spectrally sensitive in various regions of the electromagnetic spectrum and possess essential contact properties. These requirements are met by multicomponent binary semiconductor compounds of the A_2B_6 type, formed through the chemical bonding of elements from Group II A_2 (Zn, Cd, Hg) and Group VI B_6 (O, S, Se, Te) of the periodic table of elements. Additionally, multicomponent compounds may consist of a mixture of binary semiconductors, such as $(A_2^1B_6) + (A_2^2B_6)$ [1], as well as $(A_2B_6^1) + (A_2B_6^2)$, where A_2^1 and A_2^2 represent different Group II elements, and B_6^1 and B_6^2 belong to Group VI of Mendeleev's periodic table.

Cadmium sulfide (CdS) and zinc sulfide (ZnS) belong to the A_2B_6 semiconductor family, are direct bandgap materials, and are used in various optoelectronic devices, including solar cells [2–6], transistors [7–11], light-emitting diodes (LEDs) [12–14], photocatalysis [15–16], and water-splitting devices [17].

The ternary semiconductor chemical alloy $Zn_xCd_{1-x}S$ [18], also characteristic of A_2B_6 semiconductors, exhibits variable optical and photoelectric properties in its photoactive layer due to the modification of Zn and Cd content in the alloy $Zn_xCd_{1-x}S$ (where $x = Zn/(Zn + Cd)$), leading to variations in the photoelectric characteristics of actual photosensitive structures [19-20]. The bandgap width (E_G) increases with the growth of x, ranging from 2.44 eV ($x = 0, CdS$) to 3.56 eV ($x = 1, ZnS$) [21]. As E_G changes, the spectral sensitivity of $Zn_xCd_{1-x}S$ layers and the structures based on them can vary within the wavelength range of electromagnetic radiation from 500 nm to 330 nm [22,23]. $Cd_{1-x}Zn_xS$ layers can be grown using methods such as chemical bath deposition [19–21, 24], sublimation in a quasi-closed volume [25], spray pyrolysis [18,26], hydrothermal synthesis [27], and chemical transport reactions [28-29]. The synthesized layers have been utilized in solar cells [19-20, 24-25, 31] and photodetectors [27, 30, 32].

In contrast to the methods previously mentioned, the chemical vapor transport (CVT) method [33-34] with hydrogen as the carrier gas enables the synthesis of polycrystalline layers with relatively large crystallite sizes, thereby significantly extending the lifetimes of nonequilibrium photogenerated charge carriers [28]. In this method, the synthesis of the semiconductor material occurs as a result of chemical reactions between elements in the vapor phase within a gas flow on the substrate surface. The advantage of synthesizing A_2B_6 compounds from the vapor phase via chemical transport reactions lies in the ability to obtain semiconductor materials with varied properties by controlling the temperatures of both the evaporators and the substrate during the growth of the photoactive layer. This allows for the production of high-quality crystals, very close to stoichiometry, and enables the synthesis of crystals in various modifications at low temperatures.

Cite as: R.R. Kabulov, D.B. Istamov, K.T. Suyarov, F.A. Akbarov, East Eur. J. Phys. 1, 286 (2026), https://doi.org/10.26565/2312-4334-2026-1-33

Currently, a critical issue is the alignment of the wide-bandgap front buffer layer of solar cells with their photoactive layer, not only in terms of the energy band diagram but also structurally, by matching the crystal lattice constants. This alignment would increase the conversion efficiency of the solar cell. In thin-film solar cells and photovoltaic modules such as $CdTe$ and $CIGS$, CdS layers are used as the buffer layer due to their compatibility with electron affinity (χ) and lattice constant (a_0). However, in CdS-based structures, the spectral sensitivity (S) deteriorates in the spectral region $hv > E_{gCdS}$. To improve S, it is necessary to use a buffer layer with a wider bandgap, such as ZnS. However, replacing CdS with ZnS reduces efficiency due to significant differences in χ and a_0. Thus, developing and studying $Zn_xCd_{1-x}S$ layers with bandgaps adjustable between ZnS and CdS is highly desirable. Furthermore, for registration and measurement equipment, photosensitive semiconductor structures are required with maximum spectral sensitivity in the near-ultraviolet range. The main aim of this research, therefore, was to create and investigate the spectral sensitivity and photocurrent characteristics of a photosensitive semiconductor structures based on $Zn_xCd_{1-x}S$ layers, where the bandgap could be varied (graded layer).

In this work, the synthesis of the $Zn_xCd_{1-x}S$ semiconductor compound was carried out using the chemical vapor transport method, with two separate evaporators for ZnS and CdS precursors in a gas flow [33-34]. To prevent the contamination of the growing $Zn_xCd_{1-x}S$ layer with uncontrolled impurities, the evaporators underwent thermal annealing, as did the molybdenum (Mo) substrates [35-36].

METHODS AND MATERIALS

To achieve the research objective, we synthesized the $Zn_xCd_{1-x}S$ semiconductor solid alloy, designed to have maximum photosensitivity in the short-wavelength range of the electromagnetic spectrum, using the chemical vapor transport method in a hydrogen carrier gas flow.

Figure 1 shows the setup for growing $Zn_xCd_{1-x}S$ solid solutions by the chemical vapor transport method in a hydrogen carrier gas flow: (a) from separate evaporation sources (ZnS and CdS), (b) the temperature gradient of the setup, and (c) the photodetector design with an $Au - Zn_xCd_{1-x}S - Mo$ structure.

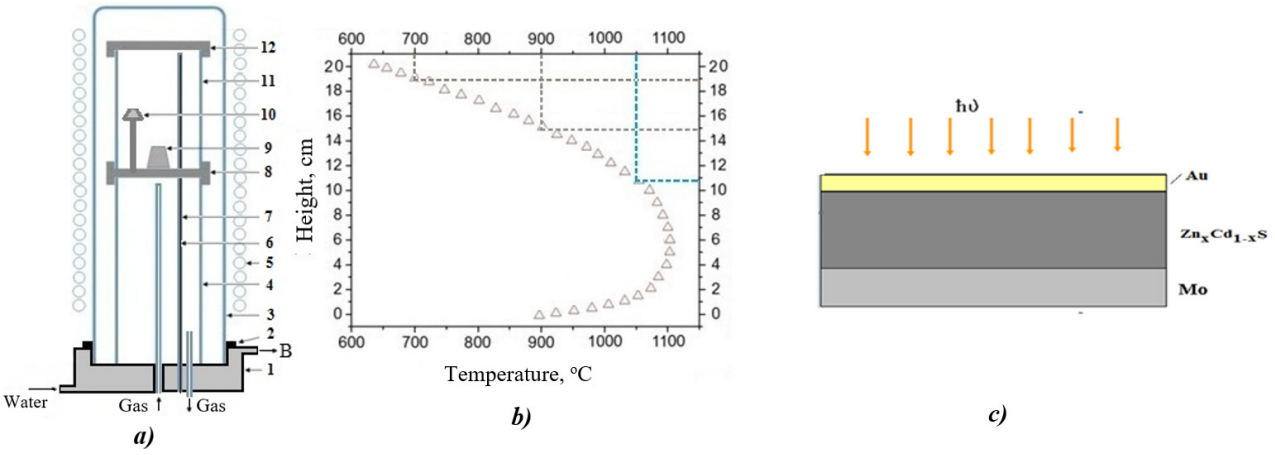

Figure 1. (a) Installation for growing the $Zn_xCd_{1-x}S$ chemical compound using the method of chemical transport reactions in a flow of hydrogen carrier gas from individual evaporation sources (ZnS and CdS), (b) temperature calibration of the installation, and (c) design of a photosensitive semiconductor structure with the $Au - Zn_xCd_{1-x}S - Mo$ configuration

At the top of the reactor, inside an inner quartz sleeve (11), are holders with substrates (12). The outer reactor casing (3) is mounted on a water-cooled flange (1), with a sealing gland (2) ensuring the reactor's airtightness. The carrier gas is supplied and vented through ports located in the lower section of the cooled flange. The quartz cup (11) is connected to a quartz stand (4) and a graphite adapter (8). The substrate temperature is measured by a thermocouple (6), which is situated within a movable quartz tube (7) affixed to the flange by a gland. Simultaneously, the quartz tube (7) serves as a fixture for the substrates. A furnace (5) is used to heat the reactor. Figure 1c illustrates the design of the fabricated photodetector with the $Au - Zn_xCd_{1-x}S - Mo$ structure. The synthesis process of the semiconductor solid solution layers was carried out on a molybdenum (Mo) substrate, approximately 150 μm thick, where Mo simultaneously served as the bottom electrical contact.

The creation of the photodetector included the preparation of substrates and initial ZnS and CdS powders. This process removed organic and inorganic contaminants as well as surface oxide layers. During the layer growth process, hydrogen purified of oxygen was used, employing the catalıoytic hydrogenation method with a chromium-nickel catalyst.

In Figure 1c, the design of the created photodetector is shown, on which investigations of photoelectric characteristics, such as spectral sensitivity [37] (Fig. 2) and photocurrent characteristics, specifically the short-circuit current versus open-circuit voltage dependency [38] (Fig. 3), were subsequently conducted.

As shown in Figure 1c, the fabricated photodetector had an $Au - Zn_xCd_{1-x}S - Mo$ structure. The photoactive $Zn_xCd_{1-x}S$ layer was approximately 10 μm thick. A semitransparent gold (Au) layer, 50 Å thick, served to create a

Schottky barrier and established an internal built-in potential generated by the difference in electron work functions between the contacting materials Au and $Zn_xCd_{1-x}S$. The gold layer also acted as the front electrical collecting contact for the photosensitive structure. The semitransparent Au contact layer was created by thermal vacuum evaporation of Au at a vacuum level of $10^{-5}\ Torr$. The effective area of the $Au - Zn_xCd_{1-x}S - Mo$ structural photodetector was $0.785\ cm^2$.

For investigating the spectral dependence of sensitivity, we utilized a research system consisting of a ZMR-3 mirror monochromator and a combined digital device (Sh-300), enabling the study of the spectral response of the photosensitive structure in the wavelength range of monochromatic radiation from $300\ nm$ to $2500\ nm$, with an accuracy of ± 10 nm for λ, 0.01% for current, and 0.1% for voltage. Monochromatic radiation penetrated the photoactive $Zn_xCd_{1-x}S$ layer through the semitransparent front Au contact, generating nonequilibrium photogenerated electron-hole pairs. These pairs were separated by the built-in electric field of the Schottky barrier ($Au/n - Zn_xCd_{1-x}S$) and were registered by the Sh-300 digital device, whose input contacts were connected to the structure's current-collecting contacts.

It is known that the photovoltaic characteristics of thin-film polycrystalline photodiodes are similar to those of $p - n$ junction photodiodes made from monocrystalline semiconductors. Specifically, the short-circuit current (J_{sc}) and open-circuit voltage (V_{oc}) increase with the rising power (P) of the incident light. J_{sc} increases linearly with P, while V_{oc} increases sublinearly in a logarithmic fashion with P [41]. The light current-voltage characteristic ($I - V$ curve), the J_{sc} (V_{oc}) dependence for $p - n$ junction photodiodes, can be expressed by formula (1) [42]:

$$V_{oc} = \frac{nkT}{q}\left(ln\frac{I_{sc}}{J_0} + 1\right), \tag{1}$$

where, n is the diode ideality factor, J_0 is the diode saturation reverse current, k is the Boltzmann constant, and q is the electron charge. The similarity in the photovoltaic properties of various photovoltaic structures (such as $p - n$ junctions, Schottky barriers, and heterostructures) mentioned above suggests that the electricity generation process under electromagnetic radiation is due to the internal electric potential of the $p - n$ junction.

The dependence of the photogenerated short-circuit current (J_{sc}) on the open-circuit voltage (V_{oc}) was studied under monochromatic illumination at different wavelengths: $\lambda_1 = 390\ nm\ (UV)$, $\lambda_2 = 460\ nm$ (blue), and $\lambda_3 = 500\ nm$ (green). The Sh-300 combined digital device was used to register the values of the photogenerated J_{sc} and V_{oc}. Its input contacts were connected to the structure's current-collecting contacts, with measurement precision at 0.01% for current and 0.1% for voltage. Since the $Zn_xCd_{1-x}S$ semiconductor layer will have different absorption coefficients (α) at various wavelengths (λ), investigating the photocurrent characteristics will provide valuable information about the photoactive layer's performance in the $Au - Zn_xCd_{1-x}S - Mo$ photodetector structure.

RESULTS AND DISCUSSION

Figure 2 presents the experimental results of the spectral photoresponse (S, in relative units) of the $Au - Zn_xCd_{1-x}S - Mo$ structure, measured at $T = 300\ K$. It is evident that the photoresponse of the fabricated $Au - Zn_xCd_{1-x}S - Mo$ structure spans the spectral range from $300\ nm$ to $500\ nm$, covering the ultraviolet region to the green part of the visible spectrum. The maximum sensitivity region is located near the wavelength of $360\ nm$.

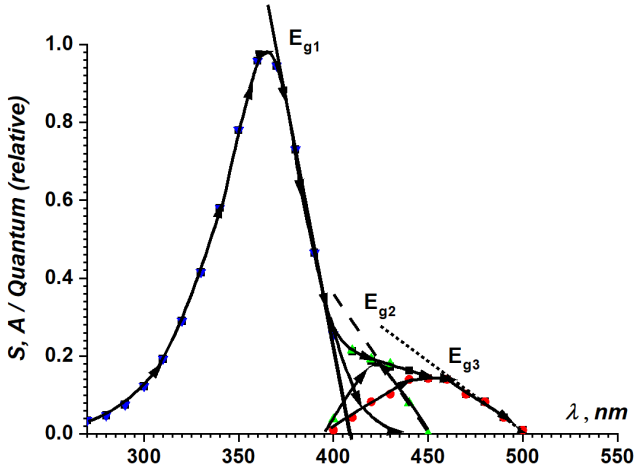

Figure 2. Spectral sensitivity of the $Au - Zn_xCd_{1-x}S - Mo$ structure, at $T = 300K$

To obtain the $Zn_xCd_{1-x}S$ layer with the spectral sensitivity shown in Figure 2, the following technological process parameters were applied: substrate temperature $T_{sub} = 923\ K$. The temperature of the evaporator for CdS powder during the entire process was maintained at $T_{evap,CdS} = 1023\ K$, and the hydrogen flow rate was set between $1.5 - 2\ L/hour$. The ZnS evaporator temperature ($T_{evap,ZnS}$) was varied throughout the process. The complete growth process for the $Zn_xCd_{1-x}S$ layer took approximately 30 minutes.

In the initial 5 minutes, $T_{evap,\,ZnS}$ was kept at around 1173 K for the next 5 minutes, it was raised to 1223 K and in the final 20 minutes, it was held at 1348 K During the first 5 minutes, due to the significantly lower evaporation temperature of CdS compared to ZnS, the growth of the $Zn_xCd_{1-x}S$ layer on the molybdenum substrate surface primarily occurred with a higher CdS content. In the subsequent 5 minutes, the temperature of the ZnS evaporator was increased by 323 K leading to the growth of a $Zn_xCd_{1-x}S$ layer with a relatively higher ZnS content. For the final 20 minutes, the ZnS evaporator temperature remained relatively high, and, as evident from Figure 2, the highest spectral sensitivity was achieved in a layer with a larger bandgap.

The experimental results of the spectral photoresponse dependence (Fig. 2) were analyzed using the photoresponse method [39,40]. Gaussian spectral sensitivity profiles of the layers contributing to the overall spectral sensitivity of the photosensitive structure were examined, considering the long-wavelength sections, and the bandgap widths of the layers formed during changes in $T_{evap,\,ZnS}$ were estimated. It was concluded that three photoactive $Zn_xCd_{1-x}S$ semiconductor layers with bandgaps of $E_{g1} \approx 3.05 \pm 0.05\ eV$, $E_{g2} \approx 2.75 \pm 0.05\ eV$ and $E_{g3} \approx 2.45 \pm 0.05\ eV$ contribute to the formation of the spectral sensitivity dependence of the $Au - Zn_xCd_{1-x}S - Mo$ photodetector structure. The photoactive $Zn_xCd_{1-x}S$ layer in the $Au - Zn_xCd_{1-x}S - Mo$ photodetector consisted of three $Zn_xCd_{1-x}S$ layers with three distinct x values: $x_1 \approx 0.6$, $x_2 \approx 0.38$, $x_3 \approx 0$ [1].

The experimental light $I - V$ characteristics, that is, the dependence of J_{sc} on V_{oc}, are presented in Figure 3. As mentioned earlier, the light $I - V$ characteristics of the $Au - Zn_xCd_{1-x}S - Mo$ photodetector structure were investigated under monochromatic illumination at wavelengths $\lambda_1 = 390\ nm$ (1), $\lambda_2 = 460\ nm$ (2), $\lambda_3 = 500\ nm$ (3). Due to the differences in photon energies, these monochromatic radiations are absorbed in different regions of the photoactive layer in the $Au - Zn_xCd_{1-x}S - Mo$ structure.

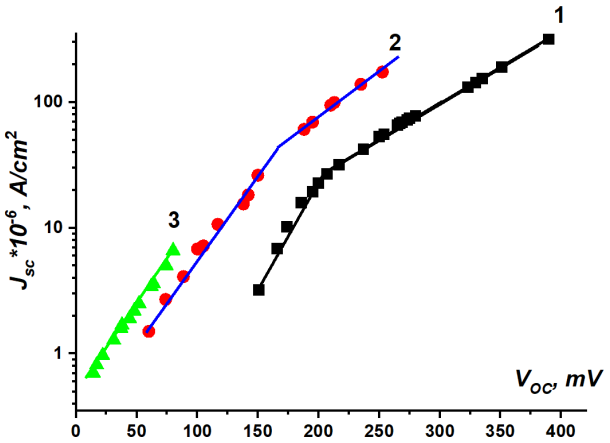

Figure 3. Light current-voltage characteristics of a photodetector with the $Au - Zn_xCd_{1-x}S - Mo$ structure, illuminated with monochromatic light with wavelengths $\lambda = 390\ nm$ (1), 460 nm (2) and 500 nm (3)

From the experimental results presented in Figure 3, it is evident that the light $I - V$ characteristics, specifically the dependence of $ln(J_{sc})$ on V_{oc} for the $Au - Zn_xCd_{1-x}S - Mo$ photodiode under illumination with different wavelengths, occupy different regions of the $I - V$ curve and display two slopes, n_1 and n_2. This contrasts with the dependence under condition 3, where the structure was illuminated with $\lambda_3 = 500\ nm$, and sufficient illumination conditions were not achieved to produce a second region with slope n_2.

The calculated results for $n_{1,2}$ and $J_{01,02}$ for different sections of the $I - V$ curve under illumination with various wavelengths are shown in the table. These results indicate that, in the first region, n_1 is close to unity for all wavelengths, suggesting a diffusion-based photogeneration mechanism and low values for J_{01}. This implies that at low illumination levels, the $Au - Zn_xCd_{1-x}S - Mo$ photodetector structure exhibits good diode characteristics [43]. As the illumination level increases, regions with n_2 and J_2 values appear. The values of n_2 and J_2 are higher compared to n_1 and J_1, indicating a degradation in the photo-detection characteristics of the $Au - Zn_xCd_{1-x}S - Mo$ photodetector due to enhanced recombination effects of nonequilibrium photogenerated charge carriers in both the quasi-neutral regions of the structure and the space-charge regions [44]. This degradation in photovoltaic characteristics suggests photo-induced formation of recombination centers within the photoactive part of the $Au - Zn_xCd_{1-x}S - Mo$ structure [45].

In the fabricated $Au - Zn_xCd_{1-x}S - Mo$ structural photodiode, the photoactive layer consists of multiple $Zn_xCd_{1-x}S$ sub-layers. During the growth of the $Zn_xCd_{1-x}S$ photoactive layer, as the evaporator temperature for ZnS changed, photoactive sub-layers were synthesized with different compositions (x), thicknesses (d), bandgaps (E_g), and concentrations of majority charge carriers (n). Radiation with $\lambda_1 = 390\ nm$ ($hv \approx 3.2\ eV$) is effectively absorbed by the layer near the front Au contact, with $E_{g1} = 3.05 \pm 0.05eV$ and $x = 0.6$. In this case, $n_1 \approx 1$, indicating a diffusion mechanism of photogeneration, and J_{01} has the lowest value, reflecting the wide bandgap of this layer. As the radiation intensity at a wavelength of 390 nm increases, the concentration of photogenerated charge carriers also increases. This leads to the formation of photo-stimulated defect states [45-46], which enhance the recombination of nonequilibrium

photogenerated carriers, increasing the diode ideality factor to $n_2 \approx 3$. This indicates that defect states form on the surface of the $Zn_xCd_{1-x}S$ photoactive layer, with J_{02} also increasing and $J_{02} > J_{01}$ [40, 41].

Table 1. Parameters of the current-voltage characteristic of the $Au - Zn_xCd_{1-x}S - Mo$ photodetector: $n_{1,2}$ - ideality coefficient of the diode and $J_{01,02}$ - the value of the reverse saturation current of the diode, when illuminated with light of different wavelengths

no.	$\lambda = 390\ nm$	$460\ nm$	$500\ nm$
n_1	1.04	1.24	1.2
n_2	3	1.4	–
$J_{01}, A/cm^2$	1×10^{-8}	2.1×10^{-7}	4.5×10^{-7}
$J_{02}, A/cm^2$	1.87×10^{-6}	1.1×10^{-6}	–

When illuminated at $\lambda_2 = 460\ nm$ $(hv \approx 2.7\ eV)$, the layers participating in photogeneration are those with $Zn_xCd_{1-x}S$ values of $x = 0.38$; $E_{g2} = 2.75 \pm 0.05eV$, and $x = 0$; $E_{g3} = 2.5 \pm 0.05\ eV$. At low radiation intensities, photogeneration occurs by a generation-recombination mechanism with $n_1 = 1.24$. The value $J_{01}(\lambda = 460\ nm) > J_{01}(\lambda = 390\ nm)$ because $E_{g1}(3.05\ eV) > E_{g2}(2.75\ eV)$. As the power of the radiation increases, photo-stimulated recombination intensifies [45-46], leading to an increase in n_2, where $n_2 > n_1$ and $J_{02} > J_{01}$.

Under illumination with $\lambda_3 = 500\ nm$ $(hv \approx 2.48\ eV)$, photons are absorbed by the thin $x = 0$ layer with $E_{g3} = 2.45 \pm 0.05eV$. As a result, the concentration of photogenerated charge carriers is relatively low. Here, $n1 \approx 1.2$, indicating that photogeneration occurs by a generation-recombination mechanism. $J_{01}(\lambda = 500\ nm) > J_{01}(\lambda = 460\ nm)$ because $E_{g2}(2.75\ eV) > E_{g3}(2.5\ eV)$. A second region with n_2 does not arise due to the low concentration of photogenerated charge carriers. The parameters of the light $I - V$ characteristics are similar to those under $\lambda = 460\ nm$ illumination, but the values of J_{sc} and V_{oc} are lower than for higher-energy photons.

Currently, the high conversion efficiency of commercially available polycrystalline thin-film photovoltaic modules, such as $CdTe$ and $CIGS$, is achieved using cadmium sulfide (CdS) as the buffer layer [47,48], with $E_g \approx 2.45\ eV$ [2]. Consequently, the spectral sensitivity of solar cells is very low in the region where $hv > 2.5\ eV$. An analysis of the energy band diagram [49] has shown that using a wider bandgap ZnS as a buffer layer does not produce the desired increase in conversion efficiency due to the difference in electron affinity between the contact materials ($\Delta\chi$). To reduce $\Delta\chi$ and further improve conversion efficiency, employing a $Zn_xCd_{1-x}S$ layer with an E_g that varies from approximately 3.1 eV to $E_g(CdS) = 2.5\ eV$ may yield the desired results. This replacement could lead to increased short-circuit current and open-circuit voltage in thin-film solar cells based on $CdTe$ and CIGS.

CONCLUSIONS

Using the chemical vapor transport method with two evaporators for ZnS and CdS precursors in a hydrogen flow, $Zn_xCd_{1-x}S$ layers were synthesized. By adjusting the ZnS evaporator temperature during the growth of the photoactive layer, an $Au - Zn_xCd_{1-x}S - Mo$ photosensitive structure was fabricated, which is sensitive in the ultraviolet and green regions of the visible spectrum and exhibits peak sensitivity at a wavelength of $360\ nm$. It was determined that the photoactive layer in the fabricated photodetector is a graded bandgap structure, consisting of $Zn_xCd_{1-x}S$ layers with $E_{g1} = 3.05 \pm 0.05eV$, $E_{g2} = 2.75 \pm 0.05eV$, and $E_{g3} = 2.45 \pm 0.05eV$. Investigations of the light $I - V$ characteristics under monochromatic illumination revealed that they are characterized by varying values of the diode ideality factor (n) and saturation reverse current (J_0). The synthesized $Zn_xCd_{1-x}S$ layer could serve as a buffer layer in thin-film solar cells, such as those based on $CdTe$ and CIGS, as a replacement for CdS, potentially enhancing both short-circuit current and open-circuit voltage in thin-film solar cells.

Acknowledgements

The authors express their gratitude to the staff of the Laboratory of Semiconductor Devices of the Physical-Technical Institute of the Academy of Sciences of the Republic of Uzbekistan for their assistance during the research process and for their advice on discussing the results of the research.

The work was carried out within the framework of the basic funding program for fundamental research of the Physical-Technical Institute of the Academy of Sciences of the Republic of Uzbekistan.

ORCID

Damir B. Istamov, https://orcid.org/0009-0007-4654-1880

REFERENCES

[1] B. Liu, J. Li, W. Yang, X. Zhang, X. Jiang, and Y. Bando, "Semiconductor Solid-Solution Nanostructures: Synthesis, Property Tailoring, and Applications," **13**(45), 1701998 (2017). https://doi.org/10.1002/smll.201701998

[2] Y.Y. Zhan, Z.B. Shao, T.H. Jiang, J. Ye, X.F. Wu, B.C. Zhang, K. Ding, D. Wu, and J.S. Jie, "Cation exchange synthesis of two-dimensional vertical Cu_2S/CdS heterojunctions for photovoltaic device applications," J. Mater. Chem. A, **8**, 789 (2020). https://doi.org/10.1039/C9TA11304E

[3] A. Bosio, G. Rosa, and N. Romeo, "Past, present and future of the thin film CdTe/CdS solar cells," Solar Energy, **175**(11), 31-43 (2018). http://dx.doi.org/10.1134/S1063783412090193

[4] V. Bermudes, "On overview on electrodeposited Cu(In,Ga) $(Se,S)_2$ thin films for photovoltaic devices," Solar Energy, **175**, 2-8 (2018). http://dx.doi.org/10.1134/S1063783412090193
[5] T. Kato, J.-L. Wu, Y. Hirai, H. Sugimoto, and V. Bermudez, "Record Efficiency for Thin-Film Polycrystalline Solar Cells Up to 22.9% Achieved by Cs-Treated Cu(In,Ga)$(Se,S)_2$," IEEE Journal of Photovoltaics, **9**(1), 325-330 (2018). https://doi.org/10.1109/JPHOTOV.2018.2882206
[6] S.-Y. Wei, Y.-C. Liao, C.-H. Hsu, C.-H. Cai, W.-C. Huang, M.-C. Huang, and C.-H. Lai, "Achieving high efficiency $Cu_2ZnSn(S,Se)_4$ solar cells by non-toxic aqueous ink: Defect analysis and electrical modeling," Nano Energy, **26**, 74-82 (2016). http://dx.doi.org/10.1134/S1063783412090193
[7] M.S. De Urquijo-Ventura, M.G.S. Rao, S. Meraz-Davila, J.A. Torres-Ochoa, M.A. Quevedo-Lopez, and R. Ramirez-Bon, "PVPS iO2 and PVP-TiO2 hybrid films for dielectric gate applications in CdS-based thin film transistors," Polymer, **191**, 122261 (2020). https://doi.org/10.1016/j.polymer.2020.122261
[8] D.B. Istamov, O.A. Abdulkhayev, Sh.M. Kuliyev, N. Abdullayev, A.Sh. Ashirov, and D.M. Yodgorova, "Temperature response curve of silicon diode temperature sensors," East Eur. J. Phys. (2), 287-291 (2025), https://doi.org/10.26565/2312-4334-2025-2-35
[9] R.R. Bebitov, O.A. Abdulkhaev, D.M. Yodgorova, D.B. Istamov, G.M. Hamdamov, Sh.M. Kuliyev, A.A. Khakimov and A.Z. Rakhmatov, "Dependence of the accuracy of the silicon diode temperature sensors for cryogenic thermometry on the spread of their parameters," Low Temperature Physics, 49(2), 277–282 (2023). https://doi:10.1063/10.0016843
[10] R.R. Bebitov, O.A. Abdulkhaev, D.M. Yodgorova, D.B. Istamov, Sh.M. Kuliyev, A.A. Khakimov, A.B. Bobonazarov, et al. "Distribution of impurities in base-depleted region of diode temperature sensor," Low Temperature Physics, 50(5), 418–424 (2024). https://doi.org/10.1063/10.0025635
[11] J. Meza-Arroyo, K.C.S. Reddy, M.G.S. Rao, F. Garibay-Martínez, M.S. de Urquijo-Ventura, and R. Ramírez-Bon, "Solution-based CdS thin film transistors with low temperature-processed Al2O3-GPTMS-PMMA as hybrid dielectric gate," Semiconductor Science and Technology, **36**, 045015 (2021). https://doi.org/10.1088/1361-6641/abe01c
[12] Y.B. Zhang, F.J. Zhang, H.Z. Wang, L. Wang, F.F. Wang, Q.L. Lin, H.B. Shen, and L.S. Li, "High-efficiency CdSe/CdS nanorod-based red light-emitting diodes," Optics Express, **27**, 7935 (2019). https://doi.org/10.1364/OE.27.007935
[13] T. Duan, J. Ai, S. Chen, G. He, X. Guo, L. Han, S. Che, and Y. Duan, "Chiral CdSe/CdS quantum dot (in rod)-light-emitting diodes with circularly polarized electroluminescence," Nano Rasearch, **15**(10), 9573-9577 (2022). https://doi.org/10.1007/s12274-022-4536-7
[14] D.B. Istamov, O.A. Abdulkhayev, and S.M. Kuliyev, "Limiting characteristics of silicon diode temperature sensors for determining the maximum temperature with specified measurement accuracy," UNEC J. Eng. Appl. Sci. **5**(1), 63-69 (2025). https://doi.org/10.61640/ujeas.2025.0507
[15] G.Z. Wang, L.X. Gong, Z.F. Li, B. Wang, W.L. Zhang, B.F. Yuan, T.W. Zhou, *et al*., "A two-dimensional CdO/CdS heterostructure used for visible light photocatalysis," Physical Chem. Chemical Physics, **22**(17), 9587-9592 (2020). https://doi.org/10.1039/D0CP00876A
[16] J.M. Hwang, M.O. Oh, I. Kim, J.K. Lee, and C.S. Ha, "Preparation and characterization of ZnS based nano-crystalline particles for polymer light-emitting diodes," Current Applied Physics, **5**(1), 31-34 (2005). https://doi.org/10.1016/.j.cap.2003.11.075
[17] X.C. Yu, Q.Q. Xing, X.P. Zhang, H.L. Jiang, and F.R. Cao, "Photoelectrochemical water splitting using TiO_2 nanorod arrays coated with Zn-doped CdS," Journal of Materials Science, **56**(18), 11059 (2021). https://doi.org/10.1007/s10853-021-06008-8
[18] S. Joishy, DD.N. Hebbar, S.D. Kulkarni, K.G. Rao, and B.V. Rajendra, "Band structure controlled solid solution of spray deposited Cd1-xZnxS films: investigation on photoluminescence and photo response properties," Physica B Condensed Matter, **586**, 412143 (2020). https://doi.org/10.1016/j.physb.2020.412143
[19] K.M. McPeak, B. Opasanont, T. Shibata, D.K. Ko, M.A. Becker, S. Chattopadhyay, H.P. Bui, *et al*., "Microreactor chemical bath deposition of laterally graded Cd1-xZnxS thin films: a route to high through put optimization for photovoltaic buffer layers," Chemistry of Materials, **25**(3), 297–306 (2013). https://doi.org/10.1021/cm3023506
[20] S.Z. Werta, O.K. Echendu, K.O. Egbo, and F.B. Dejene, "Electrochemical deposition and characterization of thin-film $Cd_{1-x}Zn_xS$ for solar cell application: the effect of cathodic deposition voltage," Thin Film Solids, **689**, 137511 (2019). https://doi.org/10.1016/j.tsf.2019.137511
[21] M. Isik, M. Terlemezoglu, S. Isik, K. Erturk, and N.M. Gasanly, "The effect of Zn concentration on the structural and optical properties of Cd1-xZnxS nanostructured thin films," J Mater. Sci: Mater. Electron. **32**, 25225–25233 (2021). https://doi.org/10.1007/s10854-021-06980-6
[22] R.R. Kabulov, L.O'. Shuhratova, K.T. Suyarov, F.A. Akbarov, D.B. Istamov. Structural, Compositional, and Photoluminescence Properties of CsPbBr3 Thin Films Grown by Single-source Thermal Vacuum Chemical Vapor Deposition. e-Journal of Surface Science and Nanotechnology 23. 364–367 (2025). https://doi.org/10.1380/ejssnt.2025-051
[23] R.R. Kobulov, M.A. Makhmudov, S.Y. Gerasimenko, and O.K. Ataboev, "Morphology and Current Transport in a Thin-Film Polycrystalline Au–$Zn_xCd_{1-x}S$–Mo Structure with Wide Photosensitivity Range in the Ultraviolet and Visible Radiation Spectral Region," Applied Solar Energy, **54**(4), 251–254 (2018). https://doi.org/10.3103/S0003701X18040084
[24] S.Z. Werta, O.K. Echendu, K.O. Egbo, and F.B. Dejene, "Electrochemical deposition and characterization of thin-film $Cd_{1-x}Zn_xS$ for solar cell application: the effect of cathodic deposition voltage," Thin Film Solids, **689**, 137511 (2019). https://doi.org/10.1016/j.tsf.2019.137511
[25] M. Zakria, A. Mahmood, A. Shah, Q. Raza, T.M. Khan, and E. Ahmed, "Tunability of physical properties of (Cd:Zn)S thin film by close space sublimation process (CSSP)," Prog. Nat. Sci. **22**, 281 (2012). https://doi.org/10.1016/j.pnsc.2012.07.006
[26] M. Shkir, M. Anis, S.S. Shaikh, M.S. Hamdy, and S. AlFaify, "Impact of Se doping on optical and third-order nonlinear optical properties of spray pyrolysis fabricated CdS thin films for optoelectronics," Appl. Phys. B, **127**, 121 (2020). https://doi.org/10.1007/s00340-020-07472-x
[27] J. Mathew, S. Devasia, S. Shaji, and E.I. Anila, "Metal–semiconductor–metal visible photodetector based on Al-doped $(Cd:Zn)$S nano thin films by hydrothermal synthesis," Optik, **241**, 166878 (2021). https://doi.org/10.1016/j.ijleo.2021.166878
[28] Sh.A. Mirsagatov, A.K. Uteniyazov, and A.S. Achilov, Physics of the Solid State, **54**, (2012). http://dx.doi.org/10.1134/S1063783412090193

[29] N.K. Abrikosov, V. F. Bankina, L.V. Poretskaya, L.E. Shelimova, and E.V. Skudnova, "AIIBVI Compounds," in: Semiconducting II–VI, IV–VI, and V–VI Compounds, (Springer Science+Business Media, New York, 1969), pp.1-64. https://doi.org/10.1007/978-1-4899-6373-4_1
[30] S.Yu. Pavelets, Yu.N. Bobrenko, T.V. Semikina, B.S. Atdaev, G.I. Sheremetova, and M.V. Yaroshenko, "Ultraviolet sensors based on $Zn_xCd_{1-x}S$ Solid solutions," Ukrainian Journal of physics, **64**(4), 308 (2019). https://doi.org/10.15407/ujpe64.4.308
[31] D. Lilhare, and A. Khare, "Temperature dependent characterizations of chemically deposited $(Cd_x$-$Zn_{1-x})S$ nanocrystalline films for solar cell applications," Optical Materials, **108**, 110385 (2020). https://doi.org/10.1016/j.optmat.2020.110385
[32] B. Barman, K.V. Bangera, G.K. Shivakumar, "$Zn_xCd_{1-x}S$ thin films: A study towards its application as a reliable photodetector," Superlattices and Microstructures, **137**, 106349 (2020). https://doi.org/10.1016/j.spmi.2019.106349
[33] Sh.A. Mirsagatov, and A.A. Mavlonov, "High Efficiency UV Photocells Based on $Zn_xCd_{1-x}S$ Solid Solutions," Applied Solar Energy, **48**(1), 51–54 (2012). https://doi.org/10.3103/S000 3701X12010100
[34] R.R. Kobulov, M.A. Maxмudov, and S.Yu. Gerasimenko, "Fabrication and investigation of ultravialet Au-ZnxCd1–xS-Mo-structures," Applied Solar Energy, **53**(1), 10-12 (2017). https://doi.org/10.3103/S0003701X1701008X
[35] Sh.A. Mirsagatov, A.Yu. Leiderman, and O.K. Ataboev, "Mechanism of Charge Transfer in Injection Photodiodes Based on the In–n+CdS–*n*CdS_xTe_{1-x}–*p*$Zn_xCd_{1-x}Te$–Mo Structure," Physics of the Solid State, **55**(8), 1635–1646 (2013). https://doi.org/10.1134/S1063783413080192
[36] R.R. Kobulov, M.A. Maxмudov, and S.Yu. Gerasimenko, "Fabrication and investigation of ultravialet Au-ZnxCd1–xS-Mo-structures, Applied Solar Energy, **53**(1), 10-12 (2017). https://doi.org/10.3103/S0003701X1701008X
[37] S.M. Sze, and K.Ng. Kwok, *Physics of Semiconductor Devices*, 3rd ed., (John Wiley & Sons, Inc., Hoboken, New Jersey, 2007).
[38] M. Grandman, "*The Physics of Semiconductors*", Second Edition, (Springer – Verlag, Berlin, Heydelberg. 2010).
[39] K. Ohata, I. Saraie, and J. Tanaka, Jap. J. Appl. Phys. **12**(10), 1641-1642 (1973). https://doi.org/10.1143/jjap.12.1641
[40] Farrukh Akbarov; Rustam Kabulov; Anvar Alimov; Erkin Abduraimov; Dildora Nasirova. Dependence of output parameters of photovoltaic module based on CIGS solar cells on external temperatures. AIP Conf. Proc. 3331, 040046 (2025). https://doi.org/10.1063/5.0305885
[41] R.R. Kabulov, M.A. Makhmudov, M.U. Khajiev, and O.K. Ataboev, "The Study of Factors that Influence on the Effectiveness of the Photoconversion of n-CdS/p-CdTe Heterostructures," Applied Solar Energy, **52**(1), 61–67 (2016). https://doi.org/10.3103/s0003701x16010047
[42] S.M. Sze, "*Semiconductor Devices. Physics & Technology*", 3rd ed. (John S. Wiley & Sons, Inc., New York, 2002).
[43] R.R. Kabulov, N.A. Matchanov, and B.R. Umarov, "Features of load current–voltage characteristics of a monocrystalline silicon solar cell at various levels of solar illumination," Applied Solar Energy, **53**(4), 297–298 (2016). https://doi.org/10.3103/S0003701X16010047
[44] Sh.A. Mirsagatov, R.R. Kabulov, and M.A. Makhmudov, "Injection Photodiode Based on an *n*-CdS/*p*-CdTe Heterostructure," Semiconductors, **47**(6), 825–830 (2013). https://doi.org/10.1134/S106378261306016X
[45] R.R. Kabulov, S.Y. Gerasimenko, and F.A. Akbarov, "Effect of Solar Radiation of Different Power on the Internal Amplification of the Primary Photocurrent in Heterostructures Based on Cadmium Telluride," Applied Solar Energy, **59**(2), 118–124 (2023). https://doi.org/10.3103/S0003701X22601065
[46] A.Yu. Leiderman, and M.M. Kashaev, "Lifetime specifics of nonequilibrum carriers in photoelectric cells based on gallium arsenide obtained via the Czochralski method," Applied Solar Energy, **49**(4), 244-247 (2013). https://doi.org/10.3103/s0003701x13040105
[47] M.A. Green, "Solar cell efficiency tables (Version 60)," Prog. Photovoltaics Res. Appl. **30**, 687–701 (2022). https://doi.org/10.1002/pip.3595
[48] A.G. Komilov, R. Kabulov, B.E. Egamberdiev, Y.Z. Nasrullayev, and F.A. Akbarov, "The Result of Successive Exposure to Reverse and Forward Bias on the Electrophysical Characteristics of ZnO:Al/i-ZnO/CdS/CuIn1 –xGax(S, Se)2/Mo Structure Solar Cells," Applied Solar Energy, **58**(4), 476-481 (2022). https://doi.org/10.3103/S0003701X22040090
[49] R.R. Kabulov, "Features of a $Zn_xCd_{1-x}S$ Buffer Layer for Use in Thin-Film Solar Cells in the Context of a Literature Review," Applied Solar Energy, **56**(5), 383–387 (2020). https://doi.org/10.3103/S0003701X20050096

ОСОБЛИВОСТІ ФОТОЕЛЕКТРИЧНИХ ХАРАКТЕРИСТИК ФОТОДЕТЕКТОРА НА ОСНОВІ ШАРІВ $Zn_xCd_{1-x}S$ З МАКСИМАЛЬНОЮ ФОТОЧУТЛИВІСТЮ В УЛЬТРАФІОЛЕТОВОМУ ДІАПАЗОНІ

Р.Р. Кабулов[1], Д.Б. Істамов[1], К.Т. Суяров[2], Ф.А. Акбаров[3]
[1]*Фізико-технічний інститут Академії наук Узбекистану, Ташкент 100084, Узбекистан*
[2]*Чирчикський державний педагогічний університет, 111700 Чирчик, Узбекистан*
[3]*Ташкентський державний технічний університет, 100095 Ташкент, Узбекистан*

Робота присвячена дослідженню фотоелектричних властивостей структурованих плівок Au–$Zn_xCd_{1-x}S$–Mo, які є фоточутливими в ультрафіолетовій та видимій областях електромагнітного спектра з максимальною чутливістю в ультрафіолетовій області. Встановлено, що спектральний відгук структурованих плівок Au–$Zn_xCd_{1-x}S$–Mo залежить від температур випарників ZnS і CdS, які впливають на склад фотоактивного шару $Zn_xCd_{1-x}S$ (x = Zn/(Zn + Cd)). Зміною температури випарника ZnS під час росту шару $Zn_xCd_{1-x}S$ на молібденовій підкладці було синтезовано градієнтний шар $Zn_xCd_{1-x}S$, який формує фотоактивний шар структури. Отримана фоточутлива напівпровідникова структура проявляє чутливість в ультрафіолетовій та видимій областях спектра з максимумом в ультрафіолетовому діапазоні. Аналіз спектрального відгуку показує, що фотоактивний шар має градієнтну заборонену зону, яка зменшується від E_G = 3,05 ± 0,05 еВ до E_G = 2,45 ± 0,05 еВ. Дослідження світлових вольт-амперних характеристик за монохроматичного опромінення показало, що вони характеризуються різними значеннями коефіцієнта неідеальності діода (n) та зворотного струму насичення (J_0). Синтезований шар $Zn_xCd_{1-x}S$ може бути використаний як буферний шар у тонкоплівкових сонячних елементах, таких як CdTe, CIGS та інших, замість шару CdS, що дозволяє підвищити як струм короткого замикання, так і напругу холостого ходу тонкоплівкових сонячних елементів.

Ключові слова: *полікристалічні плівки; $Zn_xCd_{1-x}S$; спектральна чутливість; фотоелектричні характеристики; сонячні елементи; струм короткого замикання; напруга холостого ходу*